Bose-Einstein Condensation by Polarization Gradient Laser Cooling

Wenchao Xu [1,2,*] Tamara Šumarac [3,1,*] Emily H. Qiu [1,*] Matthew L. Peters [1,*] Sergio H. Cantú [1,]
Zeyang Li,[1] Adrian Menssen,[1] Mikhail D. Lukin,[3] Simone Colombo [1,] and Vladan Vuletić [1]

[1]*Department of Physics and Research Laboratory of Electronics, Massachusetts Institute of Technology,*
Cambridge, Massachusetts 02139, USA
[2]*Institute for Quantum Electronics, Department of Physics, ETH Zürich, Zürich 8093, Switzerland*
[3]*Department of Physics, Harvard University, Cambridge, Massachusetts 02138, USA*

Attempts to create quantum degenerate gases without evaporative cooling have been pursued since the early days of laser cooling, with the consensus that polarization gradient cooling (PGC, also known as "optical molasses") alone cannot reach condensation. In the present work, we report that simple PGC can generate a small Bose-Einstein condensate (BEC) inside a corrugated micrometer-sized optical dipole trap. The experimental parameters enabling BEC creation were found by machine learning, which increased the atom number by a factor of 5 and decreased the temperature by a factor of 2.5, corresponding to almost 2 orders of magnitude gain in phase space density. When the trapping light is slightly misaligned through a microscopic objective lens, a BEC of ~ 250 ^{87}Rb atoms is formed inside a local dimple within 40 ms of PGC after MOT loading.

Quantum degenerate gases provide an attractive platform for testing fundamental physics [1,2] and simulating various quantum many-body systems [3,4]. In most experiments, highly efficient laser cooling [Doppler cooling followed by polarization gradient cooling (PGC)] takes an atomic gas from room temperature to sub-mK temperatures [5,6]. At this point, the gas is trapped with a typical occupation per quantum state [phase space density (PSD)] of $\sim 10^{-6}$, limited by detrimental light-induced processes such as photon reabsorption heating and atom loss. Subsequently, to reach the degeneracy, evaporative cooling [7] is applied. The latter is a robust method requiring only favorable atomic ground state collision properties, however, the process is slow and necessarily accompanied by a reduction in atom number.

Recently, alternative optical cooling techniques have been developed that can reach the quantum degenerate regime faster [8–13]. The main obstacle to overcome is light-induced collisional loss at higher atomic densities and within the Bose Einstein condensate (BEC) [14]. For Sr atoms, which feature a narrow optical transition, Schreck and colleagues have made use of a strongly inhomogeneous trapping potential to spectrally decouple the emerging BEC from the cooling light [8], even demonstrating the first continuous creation of a BEC [9]. For alkali atoms without a convenient narrow transition, Raman cooling can be employed to mimic a narrower transition using an additional laser field to adjust the effective transition linewidth [6,15,16]. This approach has enabled laser cooling to quantum degeneracy in Rb [11,12] and Cs [17], however, such techniques require a higher degree of experimental

complexity in addition to the PGC already necessary. It has been the general consensus that optical cooling to Bose-Einstein condensation requires relatively sophisticated, finely-tuned techniques, and cannot be accomplished by PGC alone.

In this Letter, we report the direct formation of a Bose-Einstein condensate of ^{87}Rb atoms using only PGC inside a corrugated potential. The cooling is applied to atoms trapped inside a perturbed optical tweezer, which is formed by intentionally misaligning the trapping light through a high-numerical-aperture microscope objective lens. A small fraction (up to $\sim 11\%$) of the atoms ($N \sim 2500$) forms a BEC, as revealed by a bimodal and anisotropic velocity distribution observed in time-of-flight (TOF) imaging. The BEC formation was first discovered accidentally using a machine learning algorithm designed to maximize the atom number loaded into the misaligned microscopic trap. For traps created by laser beams well aligned to the microscope objective, we do not observe a condensed component, but we consistently recover condensation in traps misaligned to the microscope. Furthermore, BECs can be generated controllably using a spatial light modulator (SLM) to imprint a specklelike phase pattern, or by superposing two closely spaced traps. We believe that interference creates dimple structures in the trapping potential that lower the trap depth below the chemical potential of the system, thus facilitating local condensate formation [18–21].

Our experimental setup is shown in Fig. 1. The optical dipole trap is generated with a Gaussian laser beam ($\lambda = 808$ nm) focused to various beam waists ($w_0 = 2$–5 μm) through a
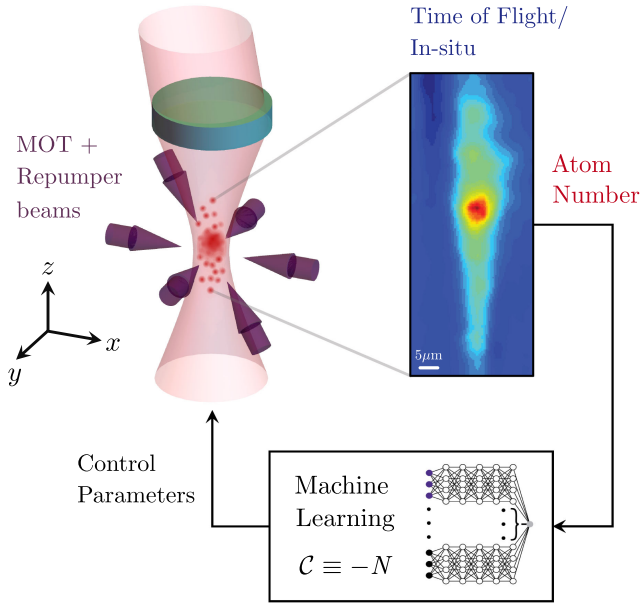
FIG. 1. Schematic of the experimental setup for direct polarization gradient cooling to Bose-Einstein condensation in a corrugated optical potential. The optical dipole trap ($\lambda = 808$ nm) is slightly misaligned on a microscope objective lens with numerical aperture NA = 0.4, resulting in small-scale corrugations of the trapping potential with waist $w_0 \approx 3.5$ μm. To maximize the phase space density and reach condensation, machine learning is used to increase the atom number loaded into the trap by tuning the trap loading and cooling parameters (see text). An absorption image (right) shows a bimodal momentum distribution. The high-density peak contains, at most, 11% of the atoms ($N = 2300$).

microscope objective lens (Mitutoyo M Plan Apo NIR B 20X 378–867–5, numerical aperture $NA = 0.4$), with the trapping beam slightly tilted ($\sim$3°) away from normal incidence on the objective. ^{87}Rb atoms are loaded into the dipole trap from a magneto-optical trap (MOT). The experimental sequence consists of a 500-ms-long MOT cooling and loading stage, followed by a 40-ms-long MOT compression stage at increased magnetic field gradient, during which atoms are loaded into the dipole trap. The dipole trap depth is typically $U/h = 8$ MHz ($U/k_B = 400$ μK), with measured radial and axial vibration frequencies of $\omega_r/(2\pi) = 18$ and $\omega_z/(2\pi) = 0.8$ kHz, respectively.

The various parameters (laser intensities and frequencies, bias magnetic fields along x, y, z, and magnetic field gradient) for the dipole trap loading during the MOT compression stage were optimized with an open-source, machine learning optimization package (M − LOOP) [22], which has been used previously for improving laser cooling to Bose-Einstein condensation [13]. In this work, we use the number of atoms loaded into the dipole trap as our cost function. We divide the 40-ms-long MOT compression stage into three time bins during which we allow M − LOOP to vary 27 parameters in total: the durations

of the time bins, the beam powers and detunings of the MOT laser on the $|5S_{1/2}, F = 2\rangle \rightarrow |5P_{3/2}, F = 3\rangle$ transition, and of the repumper laser on the $|5S_{1/2}, F = 1\rangle \rightarrow |5P_{3/2}, F = 2\rangle$ transition, the magnetic fields B_x, B_y, B_z, and the gradient of the magnetic quadrupole field. The parameters during the different time bins are connected via linear ramps, except for the laser frequencies, which are jumped in < 1 ms (see Supplemental Material [23] for details). Initial values of all parameters for the MOT compression stage are carried over from the previous MOT loading stage and were chosen by hand.

The optimized sequence obtained by the algorithm (see Supplemental Material [23]) increased the number of loaded atoms by up to a factor of 5 compared to human optimization, while simultaneously decreasing the temperature by a factor of 2.5. To increase the atomic density and reduce light-induced repulsion forces [26,27] and losses [14], the algorithm ramps down the intensity of the repumper laser by a factor of $\sim$300, which transfers most of the atoms into the $F = 1$ manifold, and reduces photon scattering. Additionally, the algorithm increases the MOT laser detuning from the $|5S_{1/2}, F = 2\rangle \rightarrow |5P_{3/2}, F = 3\rangle$ transition to -180 MHz during the final time bin to produce colder temperatures via blue-detuned PGC on the $|5S_{1/2}, F = 2\rangle \rightarrow |5P_{3/2}, F = 2\rangle$ transition [28]. The algorithm further increases the magnetic field gradient to $\sim$25 G/cm to achieve higher atomic density during dipole trap loading, while the chosen bias magnetic field positions the atomic ensemble at the dipole trap location, maximizing the loading efficiency. All of these are known techniques from human optimization. The algorithm manages to load as many as $N = 2300$ atoms into a microscopic dipole trap with beam waist $w_0 = 3$ μm, at a temperature of $T \approx 40$ μK, well below the Doppler temperature of 140 μK, while the recoil temperature is 360 nK. Note that such temperatures and densities have been achieved with PGC alone [13], while lower temperatures (e.g., 10 μK) have been reported only at the expense of lower atomic density [20]. This large atom number is remarkable given that under other loading conditions, such traps can be made to load only a single atom [29].

Following the M − LOOP-optimized trap loading, the atoms are held in the dipole trap for an additional 50–300 ms to allow the ensemble to thermalize, with typical estimated two-body collision rates of $\Gamma_c \approx 2.2 \times 10^3$ s^{-1} at peak densities $n_0 \approx 5 \times 10^{13}$ cm^{-3} of the thermal cloud. (During this 50–300 ms long thermalization stage, some evaporative cooling occurs, where 10%–30% of the atoms are lost while the temperature decreases by 10%–20%. However, this stage alone does not play a significant role for the BEC formation.) Absorption imaging *in situ* shows a local density peak inside the dipole trap, which indicates a corrugation in the optical potential of the deformed trapping beam. The TOF measurement of the atomic-cloud expansion [Fig. 2(a)] reveals that the high-density peak expands
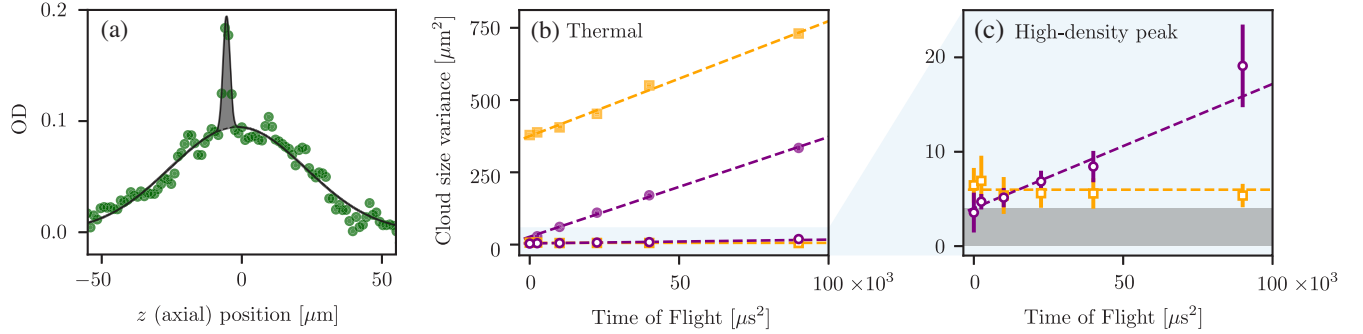
FIG. 2. (a) TOF distribution after 400 μs shows a high-density peak (gray shaded region) on top of the thermal cloud. (b) Variances of the thermal cloud (filled symbols), and (c) The high-density peak (empty symbols) as a function of the TOF. Purple and yellow markers correspond to expansion along the x (transverse) and z (axial) directions, respectively. The thermal cloud fits to temperatures of $T_x = 2K_x/k_B = 36(2)$ and $T_z = 2K_z/k_B = 42(2)$ μK along x and z, respectively, with $N = 2.7(1) \times 10^3$. The high-density peak expands anisotropically with much lower kinetic energies of expansion $2K_x^{(0)}/k_B = 1.4(2)$ and $2K_z^{(0)}/k_B < 0.2$ μK. The gray shaded region (below 4 μm²) indicates the imaging resolution.

anisotropically, and at significantly lower velocities than the thermal cloud. As shown in Fig. 2(b), the thermal cloud expands isotropically in the radial and axial directions with temperatures of $T_x = 2K_x/k_B = 36(2)$ and $T_z = 2K_y/k_B = 42(2)$ μK, while the dense peak expands anisotropically with much lower kinetic energies $2K_x^{(0)}/k_B = 1.4(2)$ and $2K_z^{(0)}/k_B < 0.2$ μK. In particular, the expansion in the axial (z) direction is too small to be resolved by the imaging system. This anisotropic expansion—well below the expansion rate of the thermal gas—is a hallmark signature of BEC formation [30]. A bimodal fit reveals an observed condensate fraction of up to 11%.

We hypothesize that interference in the aberrated trapping beam (from spurious reflections in the microscope objective) creates corrugations in the potential (local trap dimples), where the local trap potential drops below the

chemical potential [see Fig. 3(a)] such that a local condensate can form [18–21,31] (in a corrugation-free trap, the critical temperature for condensation would be 4.2 μK). The stronger confinement of the local dimple relative to the macroscopic trap enhances the local phase space density of atoms inside the dimple. When the volume of the dimple is significantly smaller than that of the macroscopic trap, the phase space density PSD_d within the dimple increases exponentially with the depth of the dimple [21]:

$$\ln(\mathrm{PSD}_d/\mathrm{PSD}) = \frac{U_d/(k_B T)}{1 + (V_d/V)e^{U_d/(k_B T)}}. \quad (1)$$

Here, U_d is the additional trap depth provided by the dimple, and V, V_d are the volumes of the macroscopic and dimple traps, respectively. The expression is an approximation assuming box-shaped trapping potentials
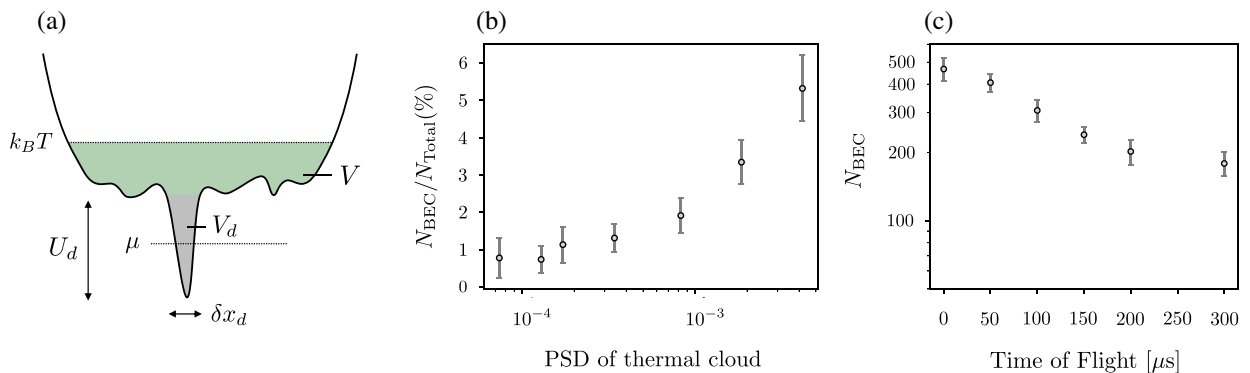

FIG. 3. (a) Corrugations in the optical potential enable BEC formation when the additional trap depth U_d drops below the chemical potential μ. Interference of the trapping beam generates diffraction-limited structures of size $\approx\lambda$, which can exponentially enhance the local PSD_d in the dimple (gray shaded region) with respect to the classical PSD of the thermal cloud (blue shaded region). (b) Fraction of atoms in the BEC peak as a function of PSD in the thermal cloud. The PSD is tuned by ramping up or down the trap power following the M − LOOP-optimized dipole trap loading. The data were taken after a TOF of 100 μs for $N = 3700(200)$, resulting in up to 200 atoms in the BEC. (c) Number of atoms in the condensate as a function of TOF delay shows fast loss as the cloud expands. In trap, however, the condensate persists for hundreds of milliseconds.

and $V_d/V \ll 1$. For smaller volume ratios V_d/V, a weaker dimple potential is sufficient to create a BEC. The largest possible increase in phase space density is $\text{PSD}_d/\text{PSD} \sim V/V_d$, obtained for a dimple depth of $U_d/(k_B T) \approx \ln(V/V_d)$. For our parameters, this implies that a volume ratio $V_d/V \lesssim 10^{-3}$ is needed, in combination with an additional dimple potential depth $U_d \approx 6.9 k_B T \approx h \times 5.5$ MHz. The smallest characteristic structure size of the interference speckle pattern can be estimated as $\delta x_d \sim \lambda/(2 \times NA) \approx 1.2\lambda$, yielding a maximum volume ratio (and hence local PSD increase) of $V/V_d \sim 2\pi^2 w_0^4/\lambda^4 \approx 1.5 \times 10^3$, matching what is required to explain the BEC formation. For the thermal gas in V, the chemical potential calculated from its temperature and atom number is approximately $U_d \approx h \times 5.5$ MHz, satisfying the BEC formation condition.

Additionally, we investigated the dependence of BEC formation on the dipole trapping beam waist w_0 and on the misalignment angle between the incident beam and the optical axis of the microscope objective. We found that the trap size is critical: while we observe BEC formation in a dipole trap with $w_0 = 3.5$ μm, no condensation was observed for waists $w_1 = 2.4$ or $w_2 = 4.5$ μm. For the smaller beam waist w_1, higher light-induced loss during the loading stage [32] into the tighter trap resulted in a smaller loaded atom number $N = 800$, and smaller phase space density PSD for the thermal cloud, which was too low to allow BEC formation. On the other hand, for the larger beam waist w_2, the dimple depth is likely too small to reach the chemical potential [Fig. 3(a)].

Once a proper dipole trap beam waist is chosen and the trap is misaligned, the formation of the BEC is reproducible and robust. We verified that BEC formation persists at various angles of misalignment, but the density peak can occur at different locations inside the trap; often, multiple high-density peaks exhibiting anisotropic expansion in TOF are observed (see Supplemental Material [23]). In contrast, when the beam is aligned at normal incidence to the microscope objective, we observe only a thermal cloud, without density anomalies or bimodal TOF distributions. Prior to the implementation of the M − LOOP algorithm, BEC formation was not observed, due to smaller loaded atom number and higher temperature obtained from human optimization.

To further verify the BEC formation, we vary the classical phase space density (PSD) of the thermal cloud and measure the corresponding condensate fraction [see Fig. 3(b)]. To change the phase space density in the trap, we use the same M − LOOP-optimized loading sequence and subsequently ramp up or down the dipole trap depth within 20 ms, and finally hold the atoms in the trap for an additional 20 ms before TOF imaging. It is evident that higher (lower) PSD yields larger (smaller) condensate fractions, as expected, since the hottest (thermal) atoms escape the trapping potential.

In order to test our dimple hypothesis and also create BECs under more controlled conditions, we introduced an SLM in the optical path of the trapping beam. We were then able to observe on-demand BEC formation for trapping beams well aligned to the optical axis of the microscope in two different configurations of the SLM. First, we used the SLM to generate two traps of 2 μm waist and observed BEC formation when the trap separation was chosen to lie in the range 3.3–3.7 μm, creating interference between the traps. Second, we also observed BEC formation when we introduced a specklelike pattern consisting of many diffraction orders generated by sine phase functions displayed on the SLM, superimposing three waves with small wave numbers (and thus small trap spacing in the atom plane) and random phase offsets. In both cases, we observed persistent BEC formation, but the condensate fractions were smaller than in the data presented in Figs. 1 and 2. However, with the capabilities introduced by an SLM, we envision possibilities to engineer more complex optical potentials in which the BEC fraction can be improved via the generation of subdiffraction–limited dimples [33,34]. A gallery of different BECs observed in various traps is shown in the Supplemental Material [23].

Notably, while the BEC persists in trap over timescales of a few hundred ms, we observe atom loss from the condensate during TOF measurements [see Fig. 3(c)]. This atom loss during TOF is consistent with two-body elastic collisions between noncondensed atoms from the larger trap and condensate atoms (see Supplemental Material [23]). In trap, the atom number in the BEC remains constant because there is a dynamic equilibrium between scattering into and out of the condensate. During TOF, however, the thermal cloud disperses quickly, and loss of atoms from the condensate cannot be recovered via elastic collisions with the thermal atoms. At short TOF, the loss of the condensate may be further enhanced due to the presence of thermal atoms confined within the dimple potential. As the thermal cloud density decreases during TOF expansion, the loss from the condensate stops. A second possible explanation for condensate loss in TOF is three-body loss [35] (see Supplemental Material [23]; note that two-body inelastic collisions should be negligible since the algorithm prepares the atoms in the $F = 1$ ground state.) However, the long BEC lifetime in trap suggests that three-body loss is unlikely to be the dominant loss mechanism on the timescale shown in Fig. 3(c).

In summary, we have, for the first time, observed the direct formation of a BEC using only regular optical molasses (PGC) laser cooling, overturning a long-held paradigm that PGC is insufficient for reaching quantum degeneracy. Given the similar properties among alkali atoms, we anticipate that this technique can be applied to other atomic species suffering from large light-induced losses. The cooling is accomplished within a duration as short as 40 ms, which is an order of magnitude faster than

that achieved in other works [10,13]. While the total cooling duration was kept fixed in this work, we envision possibilities of increasing the condensate fraction (or reducing the cooling duration) by varying the chosen cost function for the optimizer, to explore the known trade-off between atom number and temperature [13]. Additionally, the duration of MOT loading can be easily reduced by employing a 2D MOT, which would significantly improve the cycle time [36]. Combining this method with arrays of optical tweezers [37,38], it should be possible to create hundreds of small condensates simultaneously, and purify them by lowering the trap power. This may constitute, e.g., a promising starting point for atom interferometry [39,40] and other precision experiments with ultracold atoms.

[*]These authors contributed equally to this work.

[1] A. D. Cronin, J. Schmiedmayer, and D. E. Pritchard, Optics and interferometry with atoms and molecules, Rev. Mod. Phys. **81**, 1051 (2009).

[2] K. Bongs, M. Holynski, J. Vovrosh, P. Bouyer, G. Condon, E. Rasel, C. Schubert, W. P. Schleich, and A. Roura, Taking atom interferometric quantum sensors from the laboratory to real-world applications, Nat. Rev. Phys. **1**, 731 (2019).

[3] I. Bloch, J. Dalibard, and W. Zwerger, Many-body physics with ultracold gases, Rev. Mod. Phys. **80**, 885 (2008).

[4] I. Bloch, J. Dalibard, and S. Nascimbene, Quantum simulations with ultracold quantum gases, Nat. Phys. **8**, 267 (2012).

[5] J. Dalibard and C. Cohen-Tannoudji, Laser cooling below the Doppler limit by polarization gradients: Simple theoretical models, J. Opt. Soc. Am. B **6**, 2023 (1989).

[6] M. Kasevich and S. Chu, Laser cooling below a photon recoil with three-level atoms, Phys. Rev. Lett. **69**, 1741 (1992).

[7] W. Ketterle and N. V. Druten, *Evaporative Cooling of Trapped Atoms* (Academic Press, New York, 1996), pp. 181–236.

[8] S. Stellmer, B. Pasquiou, R. Grimm, and F. Schreck, Laser cooling to quantum degeneracy, Phys. Rev. Lett. **110**, 263003 (2013).

[9] C.-C. Chen, R. González Escudero, J. Minář, B. Pasquiou, S. Bennetts, and F. Schreck, Continuous Bose–Einstein condensation, Nature (London) **606**, 683 (2022).

[10] G. A. Phelps, A. Hébert, A. Krahn, S. Dickerson, F. Öztürk, S. Ebadi, L. Su, and M. Greiner, Sub-second production of a quantum degenerate gas, arXiv:2007.10807.

[11] J. Hu, A. Urvoy, Z. Vendeiro, V. Crépel, W. Chen, and V. Vuletić, Creation of a Bose-condensed gas of ^{87}Rb by laser cooling, Science **358**, 1078 (2017).

[12] A. Urvoy, Z. Vendeiro, J. Ramette, A. Adiyatullin, and V. Vuletić, Direct laser cooling to Bose-Einstein condensation in a dipole trap, Phys. Rev. Lett. **122**, 203202 (2019).

[13] Z. Vendeiro, J. Ramette, A. Rudelis, M. Chong, J. Sinclair, L. Stewart, A. Urvoy, and V. Vuletić, Machine-learning-accelerated Bose-Einstein condensation, Phys. Rev. Res. **4**, 043216 (2022).

[14] K. Burnett, P. S. Julienne, and K.-A. Suominen, Laser-driven collisions between atoms in a Bose-Einstein condensed gas, Phys. Rev. Lett. **77**, 1416 (1996).

[15] A. J. Kerman, V. Vuletić, C. Chin, and S. Chu, Beyond optical molasses: 3D Raman sideband cooling of atomic cesium to high phase-space density, Phys. Rev. Lett. **84**, 439 (2000).

[16] J. Reichel, O. Morice, G. M. Tino, and C. Salomon, Subrecoil Raman cooling of cesium atoms, Europhys. Lett. **28**, 477 (1994).

[17] P. Solano, Y. Duan, Y.-T. Chen, A. Rudelis, C. Chin, and V. Vuletić, Strongly correlated quantum gas prepared by direct laser cooling, Phys. Rev. Lett. **123**, 173401 (2019).

[18] T. Weber, J. Herbig, M. Mark, H.-C. Nagerl, and R. Grimm, Bose-Einstein condensation of cesium, Science **299**, 232 (2003).

[19] T. Kinoshita, T. Wenger, and D. S. Weiss, All-optical Bose-Einstein condensation using a compressible crossed dipole trap, Phys. Rev. A **71**, 011602(R) (2005).

[20] D. Xie, D. Wang, W. Gou, W. Bu, and B. Yan, Fast production of rubidium Bose–Einstein condensate in a dimple trap, J. Opt. Soc. Am. B **35**, 500 (2018).

[21] D. M. Stamper-Kurn, H.-J. Miesner, A. P. Chikkatur, S. Inouye, J. Stenger, and W. Ketterle, Reversible formation of a Bose-Einstein condensate, Phys. Rev. Lett. **81**, 2194 (1998).

[22] P. B. Wigley, P. J. Everitt, A. van den Hengel, J. W. Bastian, M. A. Sooriyabandara, G. D. McDonald, K. S. Hardman, C. D. Quinlivan, P. Manju, C. C. N. Kuhn, I. R. Petersen, A. N. Luiten, J. J. Hope, N. P. Robins, and M. R. Hush, Fast machine-learning online optimization of ultra-cold-atom experiments, Sci. Rep. **6**, 25890 (2016).

[23] See Supplemental Material at http://link.aps.org/supplemental/10.1103/PhysRevLett.132.233401 for details on machine-learning-optimized sequence and further analysis of the BEC, which includes Refs. [13,22,24,25].

[24] A. D. Tranter, H. J. Slatyer, M. R. Hush, A. C. Leung, J. L. Everett, K. V. Paul, P. Vernaz-Gris, P. K. Lam, B. C. Buchler, and G. T. Campbell, Multiparameter optimisation of a magneto-optical trap using deep learning, Nat. Commun. **9**, 4360 (2018).

[25] F. Dalfovo, S. Giorgini, L. P. Pitaevskii, and S. Stringari, Theory of Bose-Einstein condensation in trapped gases, Rev. Mod. Phys. **71**, 463 (1999).

[26] S. L. Cornish, N. R. Claussen, J. L. Roberts, E. A. Cornell, and C. E. Wieman, Stable ^{85}Rb Bose-Einstein condensates

with widely tunable interactions, Phys. Rev. Lett. **85,** 1795 (2000).

[27] E. A. Burt, R. W. Ghrist, C. J. Myatt, M. J. Holland, E. A. Cornell, and C. E. Wieman, Coherence, correlations, and collisions: What one learns about Bose-Einstein condensates from their decay, Phys. Rev. Lett. **79,** 337 (1997).

[28] G. Salomon, L. Fouché, P. Wang, A. Aspect, P. Bouyer, and T. Bourdel, Gray-molasses cooling of ^{39}K to a high phase-space density, Europhys. Lett. **104,** 63002 (2014).

[29] Y. H. Fung, P. Sompet, and M. F. Andersen, Single atoms preparation using light-assisted collisions, Technologies **4,** 4 (2016).

[30] M. H. Anderson, J. R. Ensher, M. R. Matthews, C. E. Wieman, and E. A. Cornell, Observation of Bose-Einstein condensation in a dilute atomic vapor, Science **269,** 198 (1995).

[31] D. Jacob, E. Mimoun, L. D. Sarlo, M. Weitz, J. Dalibard, and F. Gerbier, Production of sodium Bose-Einstein condensates in an optical dimple trap, New J. Phys. **13,** 065022 (2011).

[32] A. Fuhrmanek, R. Bourgain, Y. R. P. Sortais, and A. Browaeys, Light-assisted collisions between a few cold atoms in a microscopic dipole trap, Phys. Rev. A **85,** 062708 (2012).

[33] M. Berry, N. Zheludev, Y. Aharonov, F. Colombo, I. Sabadini, D. C. Struppa, J. Tollaksen, E. T. F. Rogers, F. Qin, M. Hong, X. Luo, R. Remez, A. Arie, J. B. Götte, M. R. Dennis, A. M. H. Wong, G. V. Eleftheriades, Y. Eliezer, A. Bahabad, G. Chen, Z. Wen, G. Liang, C. Hao, C.-W. Qiu, A. Kempf, E. Katzav, and M. Schwartz, Roadmap on superoscillations, J. Opt. **21,** 053002 (2019).

[34] E. T. F. Rogers, J. Lindberg, T. Roy, S. Savo, J. E. Chad, M. R. Dennis, and N. I. Zheludev, A super-oscillatory lens optical microscope for subwavelength imaging, Nat. Mater. **11,** 432 (2012).

[35] E. A. Burt, R. W. Ghrist, C. J. Myatt, M. J. Holland, E. A. Cornell, and C. E. Wieman, Coherence, correlations, and collisions: What one learns about Bose-Einstein condensates from their decay, Phys. Rev. Lett. **79,** 337 (1997).

[36] S. Chaudhuri, S. Roy, and C. S. Unnikrishnan, Realization of an intense cold Rb atomic beam based on a two-dimensional magneto-optical trap: Experiments and comparison with simulations, Phys. Rev. A **74,** 023406 (2006).

[37] M. Endres, H. Bernien, A. Keesling, H. Levine, E. R. Anschuetz, A. Krajenbrink, C. Senko, V. Vuletic, M. Greiner, and M. D. Lukin, Atom-by-atom assembly of defect-free one-dimensional cold atom arrays, Science **354,** 1024 (2016).

[38] D. Barredo, S. De Léséleuc, V. Lienhard, T. Lahaye, and A. Browaeys, An atom-by-atom assembler of defect-free arbitrary two-dimensional atomic arrays, Science **354,** 1021 (2016).

[39] M. Kasevich and S. Chu, Atomic interferometry using stimulated Raman transitions, Phys. Rev. Lett. **67,** 181 (1991).

[40] H. Müller, S.-w. Chiow, S. Herrmann, S. Chu, and K.-Y. Chung, Atom-interferometry tests of the isotropy of post-Newtonian gravity, Phys. Rev. Lett. **100,** 031101 (2008).